ACCSCIENCE PUBLISHING

Journal of Seismic Exploration

ARTICLE

Advances in intelligent seismic interpretation for onshore unconventional reservoirs in CNOOC: The Linxing–Shenfu gas field case

Wenlan Li[1], Qixin Li[2], Xiaowen Zheng[3], Bo Wang[1]*, Di Wang[2], and Jicai Ding[2]

[1]China United Coalbed Methane Corporation Ltd., Beijing, China

[2]China National Offshore Oil Corporation Research Institute Corporation Ltd., Beijing, China

[3]China National Offshore Oil Corporation Gas And Power Group Corporation Ltd., Beijing, China

(This article belongs to the *Special Issue: Geophysical Inversion and Intelligent Prediction Technologies for Complex Hydrocarbon Reservoirs*)

Abstract

The Linxing–Shenfu gas field, a key block for China National Offshore Oil Corporation's onshore unconventional oil and gas exploration, is characterized by complex geology that poses dual challenges to the efficiency and accuracy of traditional seismic interpretation methods. This study presents a systematic review of the application progress of machine learning, particularly deep learning, in seismic interpretation within this block since 2018. To address the specific geological characteristics and exploration needs, we developed a comprehensive intelligent interpretation workflow. This workflow integrates intelligent horizon and fault interpretation, deep clustering for seismic facies analysis, and automated identification of special geological bodies (e.g., Zijinshan igneous rock mass), enabling the accurate reconstruction of the stratigraphic framework. Furthermore, leveraging deep learning models, we achieved direct prediction of lithology, physical properties (e.g., porosity, permeability), and gas-bearing parameters, culminating in the comprehensive characterization of geological "sweet spots." Practical applications demonstrate that this intelligent interpretation workflow not only significantly enhances interpretation efficiency but also provides distinct advantages for overcoming the bottlenecks of traditional theoretical methods, such as handling low signal-to-noise ratio data, identifying thin interbeds, and predicting "sweet spots." This review provides robust support for efficient exploration and development decision-making in the Linxing–Shenfu Block.

Keywords: Unconventional reservoir; Seismic interpretation; Machine learning; Deep learning; Sweet spot

***Corresponding author:**
Bo Wang
(wangbo64@cnooc.com.cn)

Citation: Li W, Li Q, Zheng X, Wang B, Wang D, Ding J. Advances in intelligent seismic interpretation for onshore unconventional reservoirs in CNOOC: The Linxing–Shenfu gas field case. *J Seismic Explor.* 2026;35(2):025460108. doi: 10.36922/JSE025460108

Received: November 11, 2025

Revised: February 3, 2026

Accepted: February 7, 2026

Published online: March 31, 2026

Copyright: © 2026 Author(s). This is an Open-Access article distributed under the terms of the Creative Commons Attribution License, permitting distribution, and reproduction in any medium, provided the original work is properly cited.

Publisher's Note: AccScience Publishing remains neutral with regard to jurisdictional claims in published maps and institutional affiliations.

1. Introduction

The Linxing–Shenfu Block of China National Offshore Oil Corporation (CNOOC), located in the northeastern part of the Ordos Basin, covers an area of approximately 4,500 km^2. The exploration history of the Linxing–Shenfu Block comprises three

distinct phases: (i) the discovery of peripheral gas fields, (ii) initial gas field exploration, and (iii) large-scale gas field development. In 2012, CNOOC entered the Linxing–Shenfu Block after systematically comparing geological conditions between the basin margin and the interior—a strategic shift toward tight gas exploration was proposed. From 2014 to 2015, significant exploration breakthroughs were achieved in the L-4 well area, with high-yield gas flows from the Taiyuan formation and proven geological reserves exceeding 20 billion m^3, which marked the successful initial development of the tight gas reservoir.

Through a series of exploration activities, including drilling, seismic acquisition, logging evaluation, and fracture testing, geological understanding and technological innovation were deepened, gradually revealing the geological characteristics of the gas field, and resulting in rapid reserve growth. This led to the discovery of the Linxing tight gas field with a capacity of over 100 billion m^3 in 2019. Subsequently, with breakthroughs in deep coalbed methane (CBM) exploration, the exploration strategy for Linxing–Shenfu Block shifted to a dual focus on both tight gas and deep CBM,[1] with cumulative proven geological reserves of 280 billion m^3 of tight gas and 270 billion m^3 of deep CBM. In recent years, under the guidance of the whole hydrocarbon system theory in coal measures, exploration research has gradually increased, focusing on the Ordovician carbonate rocks of the Lower Paleozoic, Carboniferous bauxite rocks, and the Zijinshan igneous rock mass. These efforts are expected to pave the way for new replacement areas for future energy development.

Since 2013, through integrated planning and phased implementation, a cumulative total of 3,500 km^2 of three-dimensional (3D) seismic data has been acquired in the Linxing–Shenfu Block, achieving near-complete coverage of the exploration area. The application of 3D seismic technology has played an important role in the discovery of tight gas fields and CBM fields, as well as in the preliminary exploration of new fields such as bauxite, carbonate rocks, and igneous rocks. In terms of 3D seismic interpretation techniques, a stratigraphically facies-controlled tight-sandstone gas prediction technology system has been developed to address seismic forecasting requirements for geological and engineering sweet spots.[2] Techniques such as pre-stack waveform-controlled high-resolution inversion, geostatistical coal facies prediction, and coal body structure prediction based on multi-attribute clustering have also been explored.

Since 2018, machine learning (ML) technology, especially deep learning (DL), has seen explosive growth in cross-disciplinary research with geophysics,[3,4] and data-driven geophysical interpretation techniques have begun to gain attention. Meanwhile, CNOOC's onshore unconventional oil and gas exploration has accumulated substantial datasets characterized by diversity, homogeneity, and density. Under the guidance of new technologies and robust data support, CNOOC has developed a comprehensive ML-based seismic interpretation framework for onshore unconventional oil and gas over six years of sustained research, including horizon and fault interpretation, seismic facies clustering, special rock body characterization, and lithological, petrophysical, and gas-bearing property prediction. It encompasses the complete seismic interpretation workflow, including the establishment of stratigraphic frameworks, lithological assemblage classification, target lithology prediction, and the prediction of physical and gas-bearing properties. The combination of data-driven ML seismic interpretation technology and model-driven conventional seismic interpretation technology has achieved good results in the exploration and development of tight sandstone gas and deep CBM in the Linxing–Shenfu Block, as well as in the exploration of Ordovician carbonate rocks, Carboniferous bauxite rocks, and the Zijinshan igneous body.

2. Geological conditions and the demand for intelligent interpretation

2.1. Geological characteristics of the Linxing–Shenfu Block

The Linxing–Shenfu Block resides within the transitional zone between the Yishan Slope and the Jinxi flexural fold belt in the Ordos Basin (west of the Lishi Fault Zone), and exhibits structural characteristics comparable to those of the Yishan Slope (Figure 1).[5] Within the block, Upper Paleozoic strata exhibit an unconformable contact with Lower Paleozoic strata, marked by the absence of Middle-Upper Ordovician Series, Silurian System, Devonian System, and Lower Carboniferous Series. According to current drilling data, the stratigraphic sequence from bottom to top consists of the following: the Lower Ordovician Majiagou Formation, and the Upper Paleozoic strata exhibit continuous deposition with conformable contacts, dominated by transitional marine-terrestrial facies and continental clastic rock deposits. From base to top, the sequence includes the (i) Upper Carboniferous Benxi Formation, the Lower Permian Taiyuan and Shanxi Formations, the Middle Permian Shihezi Formation, the Upper Permian Shiqianfeng Formation, and the Lower Triassic Liujiagou Formation; (ii) the Upper Pliocene of the Neogene; (iii) the Upper Pleistocene of the Quaternary; (iv) and the Holocene of the Quaternary.

Based on the spatial relationship between the reservoirs and the source rock, the Linxing–Shenfu Block can be

divided into three sets of oil and gas systems in the vertical direction (Figure 2): (i) tight gas with a lower source and upper reservoir configuration, (ii) self-sourced CBM gas, and (iii) multi-sourced gas in carbonate and bauxite rocks with multiple reservoirs.[6,7] In addition, influenced by the thermal effects of Yanshanian magmatic intrusion in the eastern part of the basin, the Zijinshan igneous intrusion induced localized strata uplift in the central part of Linxing, resulting in the exposure of the Zijinshan alkaline complex. Its magmatic thermal effect significantly influences hydrocarbon expulsion from source rocks and the regional structural framework.[8] Additionally, the intrusion and its associated metamorphic system represent a key exploration target in the Linxing–Shenfu Block.

2.2. Demand for intelligent seismic interpretation technology

Bergen *et al.*[9] proposed three categories of ML application in geoscience: (i) automating complex predictions beyond explicit commands; (ii) modeling and inverse problems to approximate numerical simulations or capture relationships; and (iii) discovering new patterns, structures, and relationships. Based on the exploration and development demands of the Linxing–Shenfu Block, intelligent seismic interpretation technology has demonstrated significant efficacy in two aspects: labor-intensive interpretation tasks and seismic interpretation where traditional theories are inapplicable, specifically manifested in:

(i) The stratigraphic sequence interpretation across 24 geological units—including five subsections of the Ordovician Majiagou Formation, two subsections of the Carboniferous Benxi Formation, two subsections of the Taiyuan Formation, two subsections of the Shanxi Formation, eight subsections of the Shihezi Formation in the Permian, and five subsections of the Triassic Shiqianfeng Formation—has been substantially enhanced in efficiency, precision, and consistency through intelligent horizon interpretation techniques.

(ii) For the two sets of fault systems in the Upper and Lower Paleozoic, intelligent fault interpretation has been realized with the assistance of automated fault surface extraction tools, trained on a limited set of manually interpreted labels.

(iii) The essence of intelligent interpretation of stratigraphic horizons and faults is the intelligent construction of a stratigraphic framework. Within this framework, spatial segmentation and clustering of lithological assemblages across stratigraphic units are critical. Given the low signal-to-noise ratio (SNR) seismic data in the Linxing–Shenfu Block, intelligent seismic facies analysis is the most effective method for automated feature extraction.

(iv) Beyond typical sedimentary strata, the Zijinshan igneous intrusion in the eastern part of the Linxing Block significantly influences regional hydrocarbon source rocks and tectonic evolution. The 3D

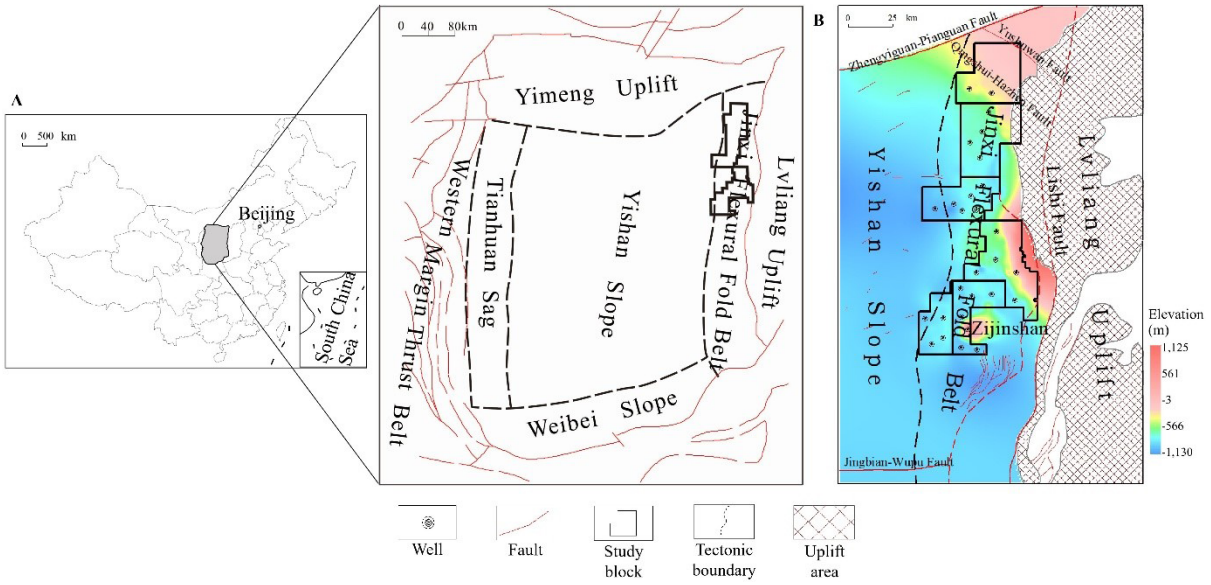

Figure 1. Geological overview of the study area. (A) Location of the Ordos Basin within China and its tectonic map. The Ordos Basin comprises six major geological units: the Jinxi flexural fold belt, the Yimeng uplift, the Yishan slope, the Weibei slope, the Tianhuan sag, and the Western Margin Thrust Belt. (B) Structural configuration of the Linxing–Shenfu Block in the eastern part of the basin.

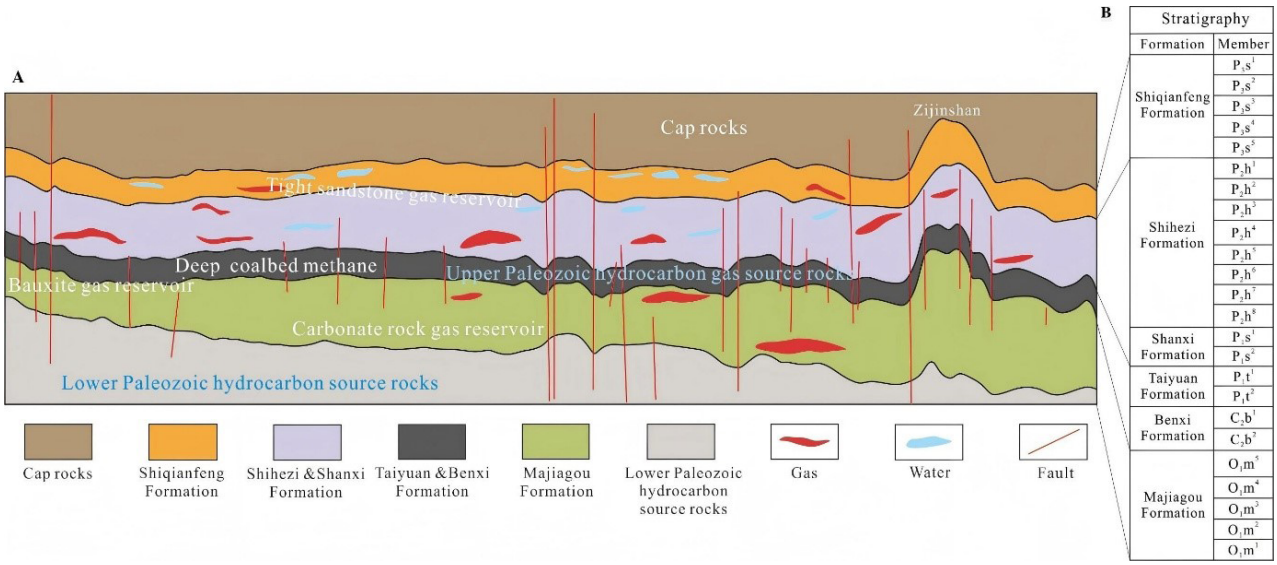

Figure 2. Geological model diagram. (A) Reservoir formation model of the entire oil and gas system in the Linxing–Shenfu Block. The system contains dual source rocks (Upper and Lower Paleozoic) and three major reservoir types (tight sandstone, bauxite, and carbonate gas reservoirs). (B) The stratigraphic sequence of the study area, comprising 24 defined geological units.

characterization of the igneous intrusion is a complex stratigraphic interpretation process with multiple *Z*-values in the vertical direction, but intelligent identification technology for special geological bodies can reduce the complexity of interpretation.

(v) The exploration and development of tight sandstone gas and CBM in the Upper Paleozoic involve predicting geological "sweet spots" (areas with high porosity, high permeability, and high gas saturation) characterized by lithology, petrophysical properties, and gas saturation. Under low porosity and permeability conditions, the overlap of seismic elastic parameters reduces their sensitivity to lithology, petrophysical properties, and gas-bearing properties. Supported by extensive well data, data-driven intelligent prediction of these parameters enables robust support for well placement optimization and reserve estimation.

3. A machine learning-driven workflow for integrated seismic interpretation

3.1. The proposed workflow and its novelty

This study presents a fully integrated and intelligent seismic interpretation workflow that systematically progresses from raw data to the characterization of "sweet spots," demonstrating a paradigm shift toward automation in subsurface analysis (Figure 3). The workflow begins with the robust, DL-enhanced identification of fundamental geological structures under low-SNR conditions, where a convolutional neural network (CNN) combined with conditional random fields (CRF) refinement and path optimization automates horizon tracking, and a U-Net++ architecture directly detects faults from seismic data, effectively replacing manual picking and traditional attribute computation. Building upon this structural framework, the workflow automatically interprets geological meaning using a deep clustering auto-encoder for seismic facies mapping and a U-Net for semantic segmentation of specific geological bodies, such as igneous rock masses, thereby bypassing subjective manual attribute selection.

Leveraging these structural and facies constraints, the system then transitions to quantitative reservoir evaluation, employing a Markov chain-constrained Bayesian classification framework for high-resolution lithofacies discrimination in thin-bedded coal-bearing strata and a geology-informed DL model for predicting physical properties such as porosity, permeability, and gas saturation. The integrated workflow culminates in a multi-layer feed-forward neural network that integrates seismic data with corrected well logs to establish nonlinear mappings between optimized seismic attributes and corrected total gas (TG) curves, effectively resolving fluid ambiguity under complex rock physics conditions and generating a continuous gas-bearing probability volume. Ultimately, all outputs, structural model, facies, lithology, physical properties, and gas content, are fused within a unified 3D model to automatically delineate composite "sweet spots."

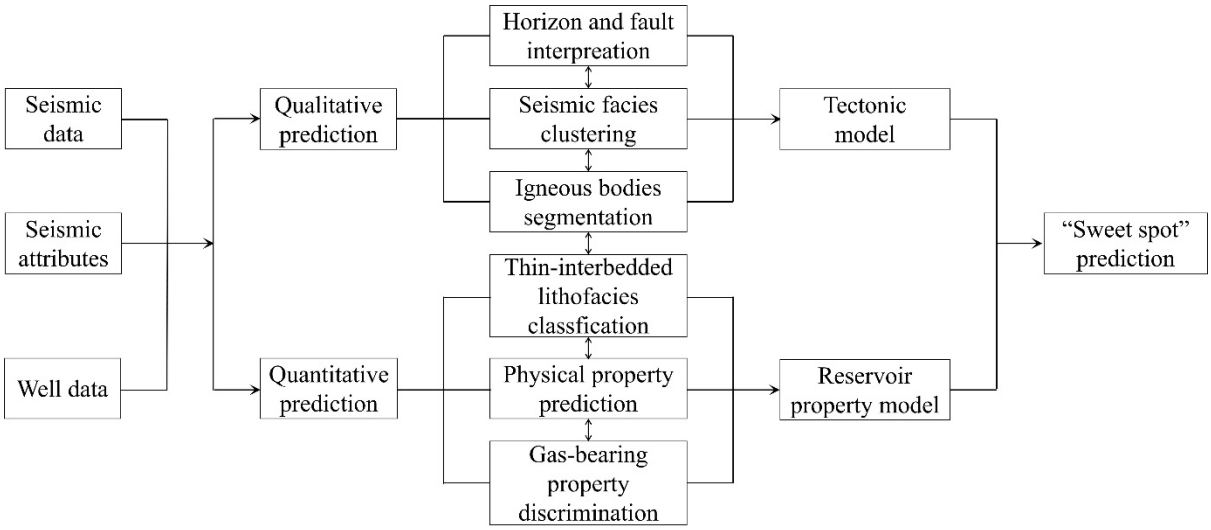

Figure 3. The machine learning-driven workflow for seismic interpretation

This innovative workflow, which establishes a systematic, automated solution, significantly reduces interpretive subjectivity and manual effort, thereby setting a new standard for data-driven reservoir characterization in geologically complex settings.

3.2. Machine learning-enhanced identification for complex geological structures

3.2.1. Robust horizon and fault interpretation under low signal-to-noise ratio

Accurate structural interpretation, encompassing both seismic horizon tracking and fault identification, is a cornerstone of subsurface model building for hydrocarbon exploration.[10] However, in the Linxing–Shenfu Block, this task is significantly impeded by low SNR and weak lateral continuity of seismic data due to heterogeneous sedimentation. Traditional horizon interpretation relies heavily on manual picking by geologists, a subjective and time-consuming process.[11] While semi-automated methods such as seed-point–guided tracking improve efficiency by correlating local waveform similarities,[12] their accuracy remains limited when encountering significant lateral waveform variations or fault disruptions. Fault interpretation traditionally relies on manual detection of seismic discontinuities, a process prone to subjectivity and constrained by data quality.[13] Although seismic attribute algorithms (e.g., coherence,[14] variance,[15] curvature,[16] and ant tracking[17]) have enhanced interpretation efficiency, they still face limitations in discriminating faults from lithological boundaries and remain computationally intensive and resolution-sensitive. This study addresses the challenge of achieving robust, automated structural interpretation under such seismically adverse conditions.

Recent advancements in DL, particularly CNN, have demonstrated significant progress in horizon interpretation[18-20] and fault detection.[21-24] Therefore, we developed an integrated workflow combining CNNs with CRF and path-optimization algorithms, forming a three-stage processing framework that progresses from local feature extraction to preliminary interpretation and, finally, to globally optimal interpretation.

In the initial stage, CNNs automatically detect features from seismic data. For horizon interpretation, CNNs are used to learn local waveform patterns, generating an initial probability volume that highlights potential horizon locations. Concurrently, for fault interpretation, specific data conditioning is applied to enhance structural edges: a multi-step structure-oriented filter is employed to suppress random noise while preserving discontinuities. Furthermore, amplitude balancing is applied to the fault-detection input to equalize energy levels across the volume, ensuring that fault features in low-amplitude or deep zones are effectively captured. Subsequently, a U-Net++ network[25] with dense skip connections executes end-to-end fault detection, producing a 3D fault probability volume. This replaces manual feature picking and traditional attribute computation with robust, initial pattern recognition.

However, the CNN's horizon predictions, while accurate locally, lack spatial coherence due to its limited receptive field. Similarly, the raw fault probability volume

may contain noise and exhibit discontinuous fault planes. Therefore, we transformed the preliminary model into a geologically consistent interpretation. For horizons, this is achieved through a synergistic combination of CRF and a path-optimization algorithm—the CRF serves as a refinement tool, and the path-optimization algorithm performs a global search to extract the most probable continuous horizon. As a discriminative probabilistic graphical model, CRF can effectively capture state–state dependencies in sequential data (e.g., continuous strata), rather than only focusing on feature mapping. We used the CNN model's output as input to the CRF model and trained it using horizon data as labels. By learning the transition probability matrix between formations, the CRF imposes strict global constraints on the predicted sequence, thereby effectively avoiding stratigraphic sequence reversals or jumps caused by local noise. For faults, the refinement involved automated extraction of fault patches from the probability volume, followed by interactive editing and validation to ensure geological reasonableness, ultimately generating fault sticks for 3D structural modeling.

Compared to seed-point auto-tracking, our method maintains continuous and accurate horizons in challenging zones (Figure 4), demonstrating improved lateral continuity and consistency with well tops. The DL-derived faults exhibited greater clarity, better vertical continuity, and more geologically reasonable geometries than those from variance or coherence attributes (Figure 5). The resulting fault probability volume enables efficient extraction of fault patches for 3D modeling (Figure 6). In summary, this integrated approach delivers structurally superior interpretations in challenging data, significantly reducing interpretive ambiguity and manual effort.

3.2.2. Seismic facies clustering with deep embedding representation

Seismic facies analysis serves as a fundamental methodology for interpreting subsurface sedimentary environments, lithological assemblages, and reservoir characteristics.[26] Traditional approaches—ranging from manual interpretation to attribute-based clustering algorithms[27] (e.g., K-means, hierarchical clustering, and

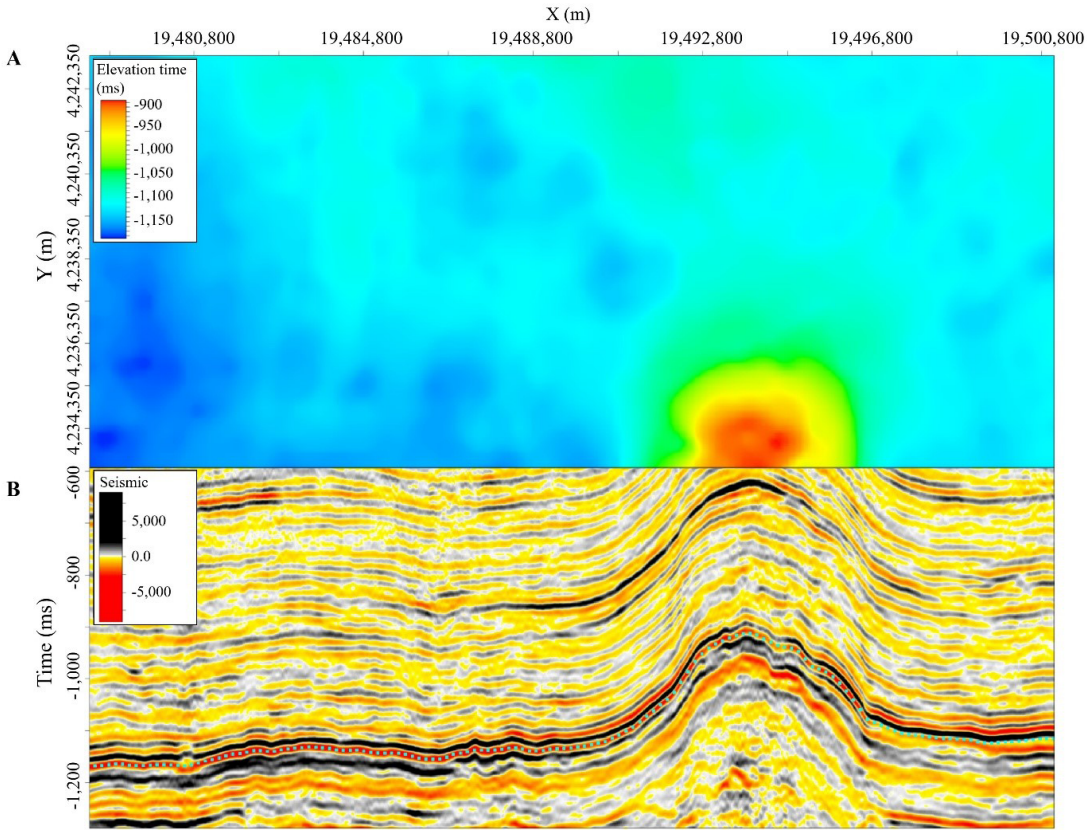

Figure 4. Deep learning-based horizon interpretation results for the Linxing Block. (A) Time-structure map derived from horizon interpretation. (B) Seismic profile showing the interpreted horizon, demonstrating consistency with primary seismic reflections.

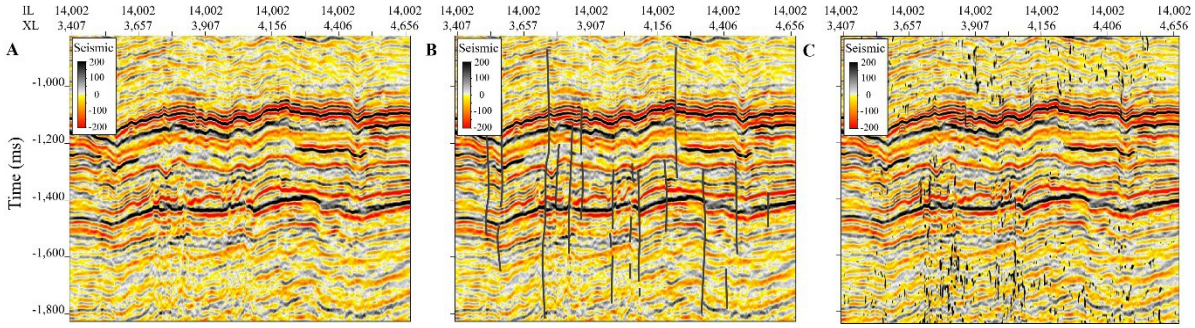

Figure 5. Comparison of fault detection methods on a representative seismic section. (A) Raw seismic profile without interpretation. (B) Fault planes extracted from the deep learning-based probability volume, demonstrating superior vertical continuity and geometric clarity. (C) Faults highlighted using the conventional variance attribute, appearing noisier and more discontinuous.

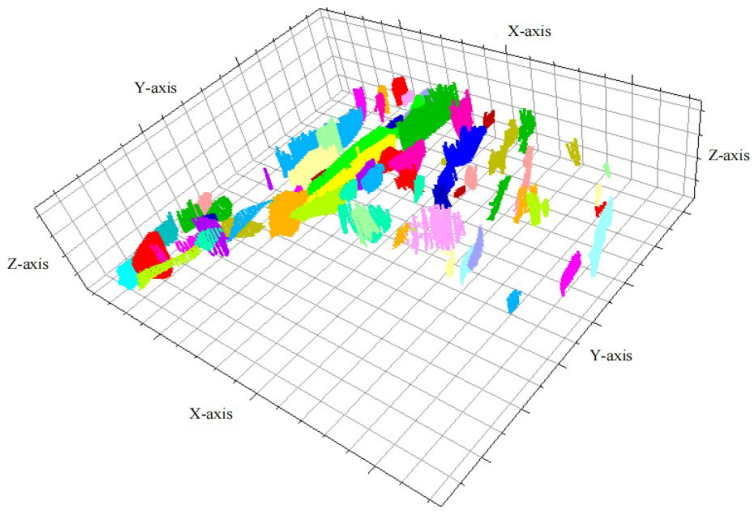

Figure 6. Polygons and fault sticks predicted using deep learning. Colors distinguish individual faults.

probabilistic clustering) and classification algorithms—inherently depend on manually designed seismic attributes.[28] This reliance introduces subjectivity, incompleteness, and redundancy, as the pre-selected attributes may not constitute the optimal feature space for facies discrimination.[29] With thin-interbedded reservoirs, such as tight sandstone, becoming key exploration targets, the rapid lithological heterogeneity within channels demands greater accuracy in seismic facies interpretation. Consequently, it is imperative to develop a fully data-driven framework. The core of this framework lies in its ability to skip manual attribute selection, directly extract optimal features from raw seismic waveforms to distinguish sedimentary facies, and achieve end-to-end mapping from waveforms to facies categories.

Crucially, unlike the structural task, data conditioning for facies clustering prioritizes amplitude preservation. We utilized seismic data processed through a true relative amplitude workflow, avoiding aggressive amplitude gain control or non-linear filtering that could distort lithological information. This ensures that the latent features extracted by the deep CNN reflect genuine sedimentary variations rather than processing artifacts.

Inspired by successful applications of deep CNNs in seismic facies analysis[30-33] and by classical mathematical transformations in geophysics (e.g., Fourier and wavelet transforms), we propose a DL-based seismic facies clustering method that balances clustering and representation performance.[34] Its key features lie in learning seismic attributes that not only restore the original signal non-destructively but are also suitable for seismic facies clustering. The architecture of our network (Figure 7) was designed to incorporate both a reconstruction loss function (L_{rec}) and a clustering loss function (L_c) during training by constructing and optimizing a joint loss function.

The implementation consisted of four sequential steps:

(i) The auto-encoder network was initially trained by minimizing the L2 norm between the input and output, thereby optimizing L_{rec} to establish fundamental feature representation capabilities.
(ii) The trained encoder was subsequently employed to transform raw seismic data into latent representations, followed by K-means clustering to initialize the cluster centers within this hidden encoding space.
(iii) Student's *t* distribution was adopted to quantify the similarity between any point in the latent space and the cluster centers, forming the target probability distribution *P*. An auxiliary target distribution *Q* was constructed to enhance intra-cluster purity. The Kullback–Leibler divergence between these distributions served as L_c, which was then back-propagated jointly with L_{rec} to optimize the network parameters. The hyperparameter λ in the joint loss function balanced the trade-off between reconstruction loss and clustering loss, and its value was determined empirically to ensure the learned representations retain sufficient geologic information while forming distinct clusters, with λ=0.1 chosen herein via validation. This selection aims to prevent gradient instability from a large λ and avoid poor cluster separation from a small λ, ultimately optimizing for both representation learning and clustering performance.
(iv) The optimized auto-encoder network was finally deployed across the seismic survey area, where each seismic trace is assigned a facies label based on minimum Euclidean distance to the cluster centers, generating the final planar seismic facies.

Validation in the Linxing–Shenfu Block demonstrates the superior performance of the proposed method compared to conventional seismic attributes. As illustrated in Figure 8, the seismic facies map generated by our network provided more geologically meaningful characterization than the root mean square amplitude attribute. The advantages are manifested in three key aspects:

(i) Enhanced channel delineation: While the root mean square amplitude attribute clearly delineated two main channels in the central study area, our method not only accurately captured these two channels but also revealed an additional channel (Face 6) in the western region, which has been confirmed by drilling data.
(ii) Improved inter-channel differentiation: The method successfully discriminated between different channel types. Specifically, the western channel (Face 6) in the central area exhibited distinct reservoir properties from the eastern channel (Face 4), with drilling data confirming differences in average gas layer thickness, porosity, and gas saturation between these facies.
(iii) Enriched geological details: The method revealed finer sedimentary features, including channel boundaries (Face 3) and local thickness variations within channel deposits (Face 2), effectively capturing the internal heterogeneity of the channel systems. These results validate the robust clustering capability and data recovery accuracy of our proposed network, establishing it as a more effective tool for seismic facies analysis and reservoir prediction in geologically complex settings.

3.2.3. Semantic segmentation of igneous intrusive bodies with limited labels

Igneous rocks and salt-related structures play multiple roles in hydrocarbon exploration, both affecting the understanding of subsurface structures and the reconstruction of sedimentary environments,[35] and also serving as significant oil and gas reservoirs. These

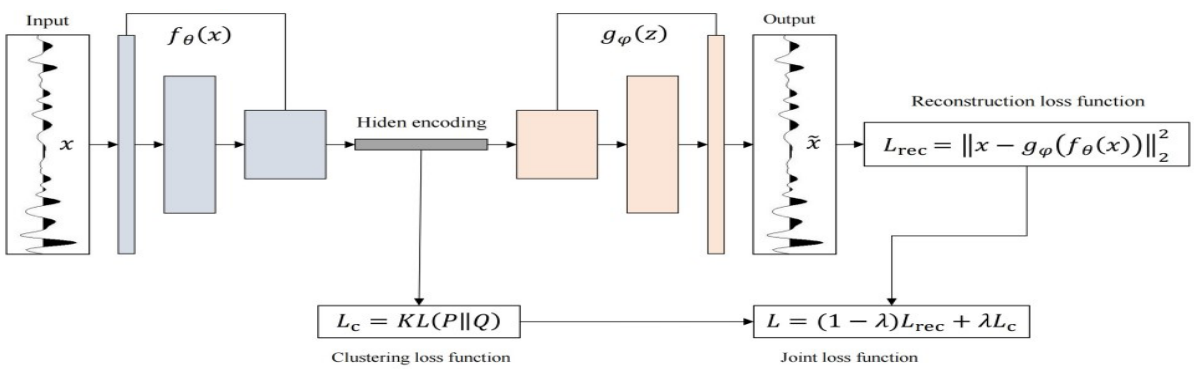

Figure 7. Structure of seismic facies deep clustering network

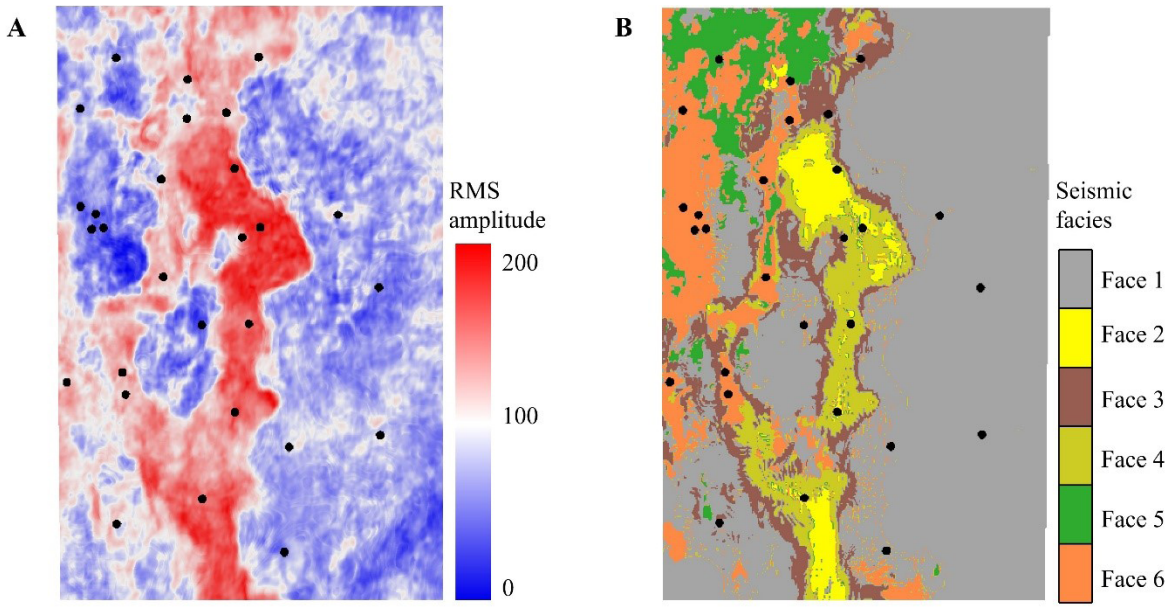

Figure 8. Comparison of seismic facies clustering results. (A) Root mean square (RMS) amplitude attribute, showing only two main channels in the central area, with no discernible internal heterogeneity. (B) Seismic facies clustering result, clearly delineating three channels and revealing internal variations. Black dots indicate well locations.

geological bodies typically exhibit strong velocity contrasts and distinct geometric configurations compared to surrounding rocks,[36] producing diverse seismic reflection patterns, including discontinuities, chaotic reflections, and amplitude variations. However, in practice, noise contamination and resolution constraints often obscure geological boundaries, complicating accurate identification. While conventional seismic attributes such as coherence, variance, and fault likelihood have been widely used for detection, they remain sensitive to non-geological discontinuities, frequently generating "fly points" in the identified boundaries and still relying on manual correction due to limited automation. Therefore, accurately characterizing the 3D spatial morphology of specific geological bodies under the constraint of limited manual labels is critical.

To address the scarcity of labeled data, a DL-based image segmentation approach using the U-Net[37-40] architecture was introduced, which treats geological body identification as a semantic segmentation task. In delineating the distribution range of the Zijinshan igneous intrusive body, seismic facies markers for igneous rock identification were first established. These markers are primarily characterized by mound-shaped, moderate to low-amplitude reflections, with localized areas exhibiting oblique reflections relative to the surrounding rocks' seismic phases and strata thickening (Figure 9). Based on these criteria, manual interpretations along only 12 main survey lines, representing approximately 7% of the total dataset, were used as training samples. These interpreted seismic profiles—where igneous rock bodies are assigned a value of 1 and non-igneous rock bodies a value of 0—paired with corresponding raw seismic profiles, served as input–output pairs to train the network. After that, a probability volume of the igneous rock body was predicted for each uninterpreted seismic profile, and the distribution range of the igneous rock body was delineated based on the probability volume. Notably, in contrast to conventional seismic attribute-based methods, which are often limited to two-dimensional planar analysis or qualitative interpretation, our deep learning approach enables the delineation of the 3D spatial extent of such complex geological bodies, thereby providing a spatially continuous and quantitative delineation of the igneous rock distribution with enhanced capability.

The trained network was applied to the entire seismic volume to generate a 3D probability model of the igneous intrusive body in the Zijinshan area. As illustrated in Figure 10, the resulting 3D carving clearly reveals two phases of igneous intrusion. According to the results from *in situ* zircon U–Pb, hornblende and biotite ^{40}Ar–^{39}Ar, and zircon and apatite fission track analyses, Zijinshan intrusive rocks primarily formed during the Late Jurassic to Early Cretaceous, when medium-deep to medium-shallow magmatic-thermal events occurred in the eastern Ordos Basin.[41-43] Within structurally weak zones of the

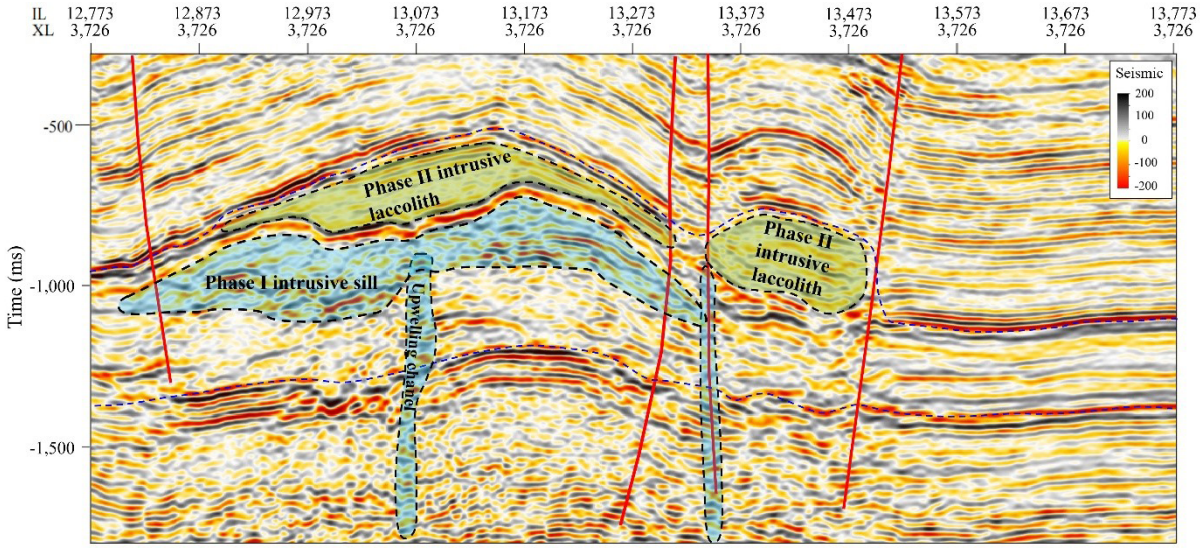

Figure 9. Manual interpretation labels for the igneous intrusive body. The red lines denote faults, the blue dashed lines represent horizons, the blue vertical features correspond to magma upwelling channels, the blue irregular shape indicates the Phase I intrusive sill, and the green irregular shape marks the Phase II intrusive laccolith.

Zijinshan area, two distinct magmatic-thermal upwelling events took place, ultimately forming an alkaline complex through mantle-derived intrusion and volcanic eruptions. Furthermore, our results successfully identify these two intrusive cycles (Figure 10).

The first phase consists of sill intrusions primarily emplaced within Ordovician strata, forming the main body of the Zijinshan igneous complex. The second phase forms two asymmetric laccoliths intruding into both Ordovician and Carboniferous layers. Laccolith 1 resulted from magma ascending along faults within the main sill body, while Laccolith 2 formed through magma intrusion along peripheral faults at the edge of the sill. From the perspective of the relationship between the thermal evolution history of the Ordos Basin and hydrocarbon accumulation, the thermal effects associated with magmatism played a crucial

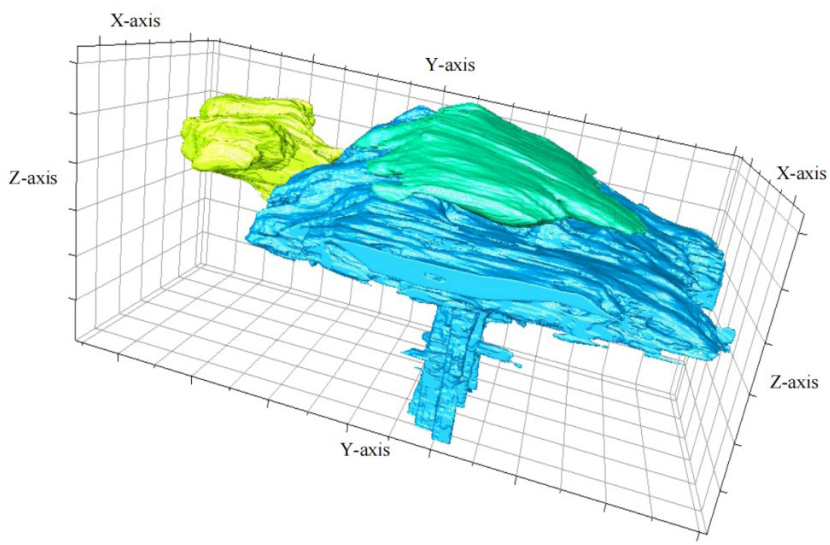

Figure 10. Three-dimensional carving results of the igneous intrusive bodies based on semantic segmentation. Blue vertical features correspond to magma upwelling channels, the blue irregular shape indicates the Phase I intrusive sill, and the green and yellow irregular shapes mark the Phase II intrusive laccolith.

role in hydrocarbon expulsion from source rocks.[44]

Additionally, the Zijinshan intrusive contact metamorphic system and its internal configuration show potential for hydrocarbon accumulation. Moreover, due to igneous intrusion and eastern marginal uplift of the basin, the Zijinshan structure zone exhibited exceptionally developed fault systems, providing effective pathways for vertical hydrocarbon migration. Therefore, delineating favorable exploration areas based on the distribution of laccoliths and sills, along with associated fault development patterns, is of significant importance for assessing the multi-gas accumulation potential in the Zijinshan area. The results confirm that the proposed method significantly enhances automated interpretation and accuracy, even with very limited training data, offering an efficient tool for characterizing special geological bodies in complex settings.

3.3. Data-driven prediction of reservoir properties

3.3.1. A Bayesian lithofacies classification framework for thin interbeds

The Linxing–Shenfu Block contains a vertically stacked sequence of marine-continental transitional coal-bearing strata, with main lithologies such as mudstone, tight sandstone, and coal. According to well logging interpretation statistics, the thinnest coal seam measures only 3 m, whereas the thickness of individual sandstone layers in the Benxi and Taiyuan Formations ranges from 2–10 m. The thickness of thin layers is far below the seismic resolution limit, thus posing a challenge to the detailed characterization of reservoirs.

In addition, coal seams exhibit low density and low P-wave impedance, resulting in strong impedance contrasts and high reflection coefficients with surrounding rocks. At low resolution, the strong seismic reflections from coal seams interfere with reflections from adjacent sandstones, resulting in strong amplitude on seismic sections and shielding sandstone reflections near the coal seams, thereby affecting seismic lithofacies identification. Therefore, reliably identifying thin sandstone layers under these constraints represents a key challenge.

Reservoir lithofacies prediction is essential in hydrocarbon reservoir characterization. Current methods commonly use elastic attributes derived from seismic inversion,[45] with techniques including discriminant analysis, Bayesian classification, neural networks, support vector machines, and K-nearest neighbor classification. Among these, Bayesian classification represents the most mature approach, integrating a seismic likelihood function with prior information from well logs to generate posterior probabilities that quantify lithological classification.[46-50] The Bayesian framework also commonly incorporates a one-dimensional Markov chain prior model, formulated as a transition probability matrix, to enforce vertical continuity in lithofacies distribution.[51,52]

Integrating geological constraints with Bayesian methodology, we developed a systematic workflow for lithofacies classification in coal-bearing strata, which mainly includes four steps:

(a) Step 1: Data conditioning and upscaling

Prior to modeling, well logs underwent rigorous quality control, including depth matching (aligning logs with seismic time using checkshot data) and outlier removal to eliminate spikes. To ensure consistency across the survey, all log curves were normalized using *Z*-score scaling. Subsequently, log curve upscaling was performed using the Backus averaging criterion to achieve precise matching between the well and seismic scales.

(b) Step 2: Optimal attribute pair selection

To enhance seismic lithology identification performance in the aliasing region of petro-physical crossplots, a Bayesian classification confusion matrix was introduced to quantify the classification ability of different attribute pairs.

(c) Step 3: High-resolution seismic inversion

To reduce the effects of strong coal seam reflections and identify thin layers, the seismic waveform indicator inversion method was used to obtain high-resolution P-wave impedance and gamma-ray data volumes. The seismic waveform indicator inversion can construct a mapping relationship between seismic traces and high-frequency components of the logging curve, widen the seismic frequency band, and considerably improve the vertical resolution.[53] It also uses horizontal changes in seismic waveforms to reflect lithological assemblage characteristics for facies-controlled constraints. The use of seismic waveforms in inversion further exploits the potential waveform characteristics and wave-group relationships of seismic data, thereby reducing the impact of strong coal-seam reflections.

(d) Step 4: Seismic attribute interpretation

To improve the continuity and accuracy of the interpreted results, a Markov chain-constrained Bayesian classification of seismic attribute volumes was performed, and probability density functions were calculated from well logging curves in step 2 using kernel density estimation, which served as likelihood functions for Bayesian classification.[54] To address the inherent class imbalance—where mudstone is the dominant background and coal/sandstone are minority classes—the Monte Carlo simulation was employed to equally expand the training samples of different lithofacies,

ensuring that each facies has the same sample size in the estimation of conditional probability density functions and in the classification evaluation.

The application in the Linxin–Shenfu Block demonstrates the method's ability to generate detailed 3D lithofacies predictions. Figure 11 shows that our approach successfully identified not only coal seams but also thin sandstone layers immediately adjacent to them. Statistically, the lithology predictions obtained by this method showed high consistency with lithology interpretations derived from well logs. The method can identify coal seams as thin as 3.3 m, and the recognition accuracy for coal seams, tight sandstone, and mudstone is 0.90, 0.86, and 0.85, respectively. The derived lithofacies volume enables the extraction of stratigraphic attributes for mapping coal distribution and characterizing sandstone reservoirs, thereby providing substantial technical support for predictive reservoir modeling.

3.3.2. Integrating geological priors in deep learning for physical property prediction

For tight sandstone and shale gas reservoirs characterized by low porosity, low permeability, and strong heterogeneity, identifying localized areas with high porosity, high permeability, and high gas saturation, commonly referred to as "sweet spots," is crucial for enhancing hydrocarbon productivity.[55] Accurate delineation of these "sweet spots" can avoid inefficient well placements and significantly improve development economics. Extensive drilling and gas test results in the Linxing–Shenfu Block indicate that high-productivity wells are typically associated with reservoirs with porosity greater than 12%, permeability exceeding 1 mD, and gas saturation above 50%. Consequently, the quantitative prediction of these "sweet spots" is our primary objective.

Conventional methods for predicting physical properties primarily include attribute analysis,[56,57] frequency-division

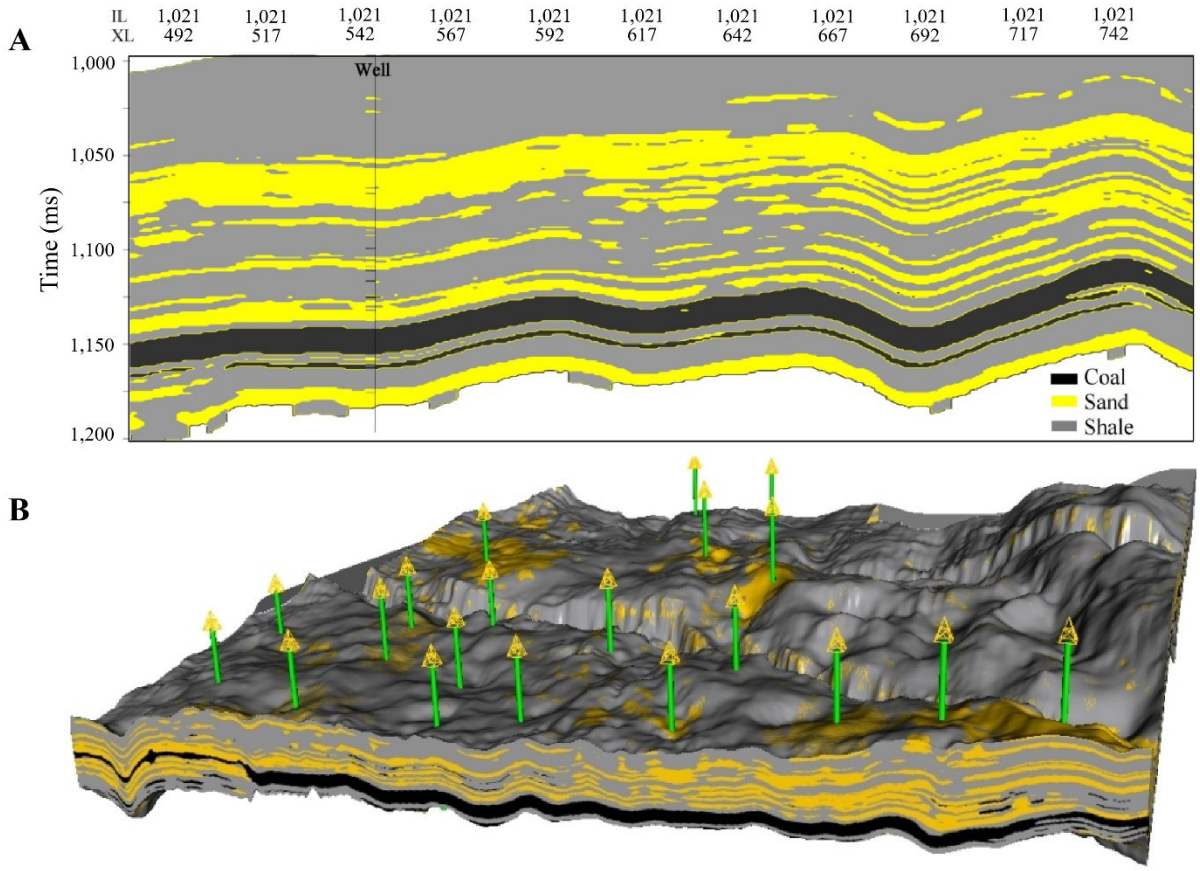

Figure 11. Lithology results based on Bayesian classification prediction, with yellow, black, and gray representing sandstone, coal, and mudstone, respectively. (A) Lithology profiles. (B) Three-dimensional lithology volume, with drilled wells indicated in green.

attribute fusion,[58] and seismic inversion.[59,60] For instance, by analyzing differences in petrophysical properties or seismic response characteristics between sweet-spot and non-sweet-spot reservoirs, inversion techniques and attribute analysis were employed to identify sweet-spot distribution. However, these traditional techniques face dual challenges. On the one hand, these methods largely rely on empirical relationships or qualitative analysis of regional data. Due to the lack of a direct analytical relationship between reservoir physical parameters and seismic data, it is difficult to establish a direct mapping between them.[61] On the other hand, our study block exhibited a significant contradictory sample phenomenon (i.e., similar seismic waveforms correspond to drastically different well log responses, or different reservoir parameters correspond to similar seismic response characteristics). This non-unique correspondence between seismic and well log data severely restricts the direct application of conventional methods, leading to unstable prediction results, insufficient vertical resolution, and an inability to meet the requirements for finely characterizing sweet-spot distribution during the development stage.[62]

In addressing such geological challenges, many researchers have turned to DL techniques—training networks to learn the implicit relationships that map seismic data to physical property parameters.[63] By constructing complex network architectures, such as CNNs, recurrent neural networks, deep belief networks, and hybrid DL networks, the complex nonlinear relationships between seismic data and reservoir parameters can be explored. This approach fully leverages the advantages of a data-driven methodology, bypasses the seismic rock physics modeling step, and improves reservoir prediction accuracy. Promising results for predicting reservoir physical properties have been achieved in areas with high well density. Building upon this, our study introduces a further improvement by innovatively proposing a DL-based technical framework integrated with geological prior constraints.[62] Specifically, our DL-based network model enhances the conventional CNN by incorporating fully connected layers. These layers integrate prior information, such as horizons and seismic facies, to resolve contradictory samples and ensure stable predictions. Simultaneously, the raw seismic data were fed into a locally connected CNN. The outputs from these two parts were then fused to produce the network's final output. The training labels (e.g., porosity, permeability, and gas saturation) were derived from log interpretations rigorously calibrated against core analysis data.

Accordingly, we constructed a training dataset using seismic data and geological prior information as inputs and the reservoir parameters (e.g., porosity, permeability, and gas saturation) from sample wells as outputs to train the network. During the screening of sample wells, we established strict geologically guided criteria, ensuring not only uniform spatial coverage across the study area but also representation of key sedimentary microfacies, including channel bars, composite channels, channel margins, and inter-channel bays, thereby guaranteeing sample balance and diversity. Application of this network in the Linxing–Shenfu Block demonstrates that the predicted physical properties not only match well with drilling data but also exhibit stronger geological consistency (Figure 12), thereby effectively delineating the distribution of "sweet spots."

3.3.3. Gas-bearing property discrimination using a multi-attribute neural network

Gas-bearing property prediction, the ultimate objective of seismic reservoir characterization, constitutes a highly non-unique problem due to limitations in seismic SNR, resolution, and complex rock physics. Conventional approaches relying on seismic attribute analysis (e.g., amplitude, frequency,[64] attenuation,[65] and amplitude-versus-offset) or seismic inversion techniques[66] exhibit limited discrimination capability for thin interbedded layers, low-SNR data, or complex lithological structures. Moreover, the complex dependence of gas-bearing properties on multiple factors, including rock physics, stratigraphic architecture, and fluid saturation, cannot be adequately captured by individual attributes or conventional analytical methods.

The eastern part of the Linxing–Shenfu Block, tectonic uplift associated with the Luliang Uplift, has led to diminished hydrocarbon generation intensity in source rocks and insufficient gas charging dynamics, resulting in widespread gas-water mixing within the Shihezi Formation. Post-stack seismic profiles showed no significant differences between gas-bearing and water-bearing layers, while rock physics analysis revealed overlapping elastic parameters. These conditions render conventional discrimination methods ineffective, making reliable gas prediction a critical challenge in this area.

The TG curve—one of the primary logging methods—contains substantial reservoir information through its amplitude values and morphological variations, serving as a direct indicator for detecting and evaluating gas-bearing zones.[67] Gas-bearing layers typically exhibit high TG values, whereas water-bearing layers show low values. While providing high vertical resolution, TG lacks lateral continuity, and seismic data exhibit opposite character. By integrating the complementary advantages of these two data types through an appropriate methodology, direct prediction of reservoir gas-bearing potential can

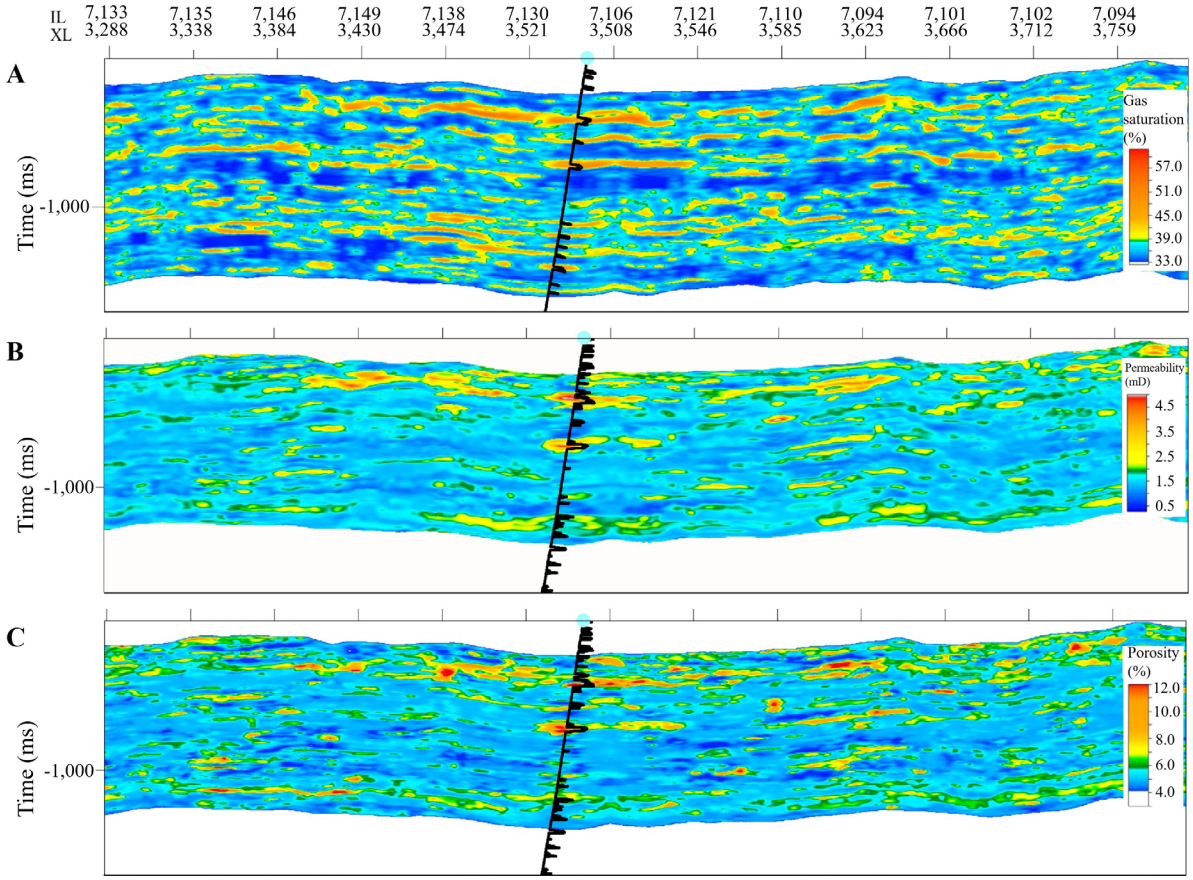

Figure 12. Prediction results of physical properties: (A) Gas saturation, (B) permeability, and (C) porosity

be achieved. DL technology enables effective integration of these complementary datasets and geological pattern recognition,[68,69] establishing nonlinear mappings between multi-attribute seismic inputs and TG responses to resolve prediction non-uniqueness.

To address these challenges, a workflow with a multi-layer feed-forward neural network was employed. The workflow initiates with standardized correction of TG from well logs, accounting for influencing factors such as drill bit diameter, drilling time, and drilling fluid density. This correction ensures that the normalized TG values reliably reflect vertical variations in gas-bearing properties while maintaining lateral comparability across the study area. Subsequently, the Hilbert transform was applied to the seismic data to extract a comprehensive set of attributes, including amplitude, frequency, and phase components within the target interval, generating a seismic attribute database. Pearson correlation coefficients were then calculated between the corrected TG and each seismic attribute at well locations. Attributes showing significant correlation with TG were retained, while those inconsistent with geological understanding were systematically eliminated. The optimized attribute set, together with the corrected TG data, served as input to a neural network. Model training was performed under the constraint of pre-stack P- and S-wave velocity ratio (Vp/Vs) inversion results to reinforce petrophysical consistency, thereby establishing a robust nonlinear mapping relationship between the multi-attribute seismic input and TG properties. This integrated approach enhances prediction reliability by jointly leveraging the complementary strengths of well logs, seismic attributes, and rock physics constraints.

The trained model was applied to the full 3D seismic volume to generate a continuous TG prediction cube. This resultant data cube enables delineation of gas-bearing distributions within the target formation, informed by structural interpretation. Notably, the TG prediction successfully identified gas zones that are indistinguishable from water-bearing layers using conventional pre-stack inversion methods, demonstrating effective gas-layer prediction even under high water-saturation conditions (Figure 13).

4. Key challenges and future directions in unconventional reservoir characterization

Based on the practices in the Linxing–Shenfu Block, several key research directions for intelligent geophysics are summarized as follows:

(i) Emphasize the core role of data quantity and quality in improving ML models: The Linxing–Shenfu Block remains in the early stage of oil and gas exploration and development, and data are still being accumulated. Through continuous data accumulation and cleaning, noise removal, and SNR improvement, the models are enabled to learn more representative geological features from purer and richer data. Moreover, iterative data utilization, that is, fine-tuning models based on feedback from prediction results after initial model training and continuous model iteration, further optimizes prediction accuracy, thereby highlighting the critical role of data quantity and quality in model optimization.

(ii) ML models should avoid excessive complexity: Compared to data from the complex physical world, geoscientific data exhibit cyclicity and low dimensionality. The design of intelligent geophysical models follows the Occam's Razor principle, that is, models should be as simple and interpretable as possible while meeting interpretation requirements. From current practice, various improved complex intelligent models provide limited improvements in efficiency and accuracy for industrial-level

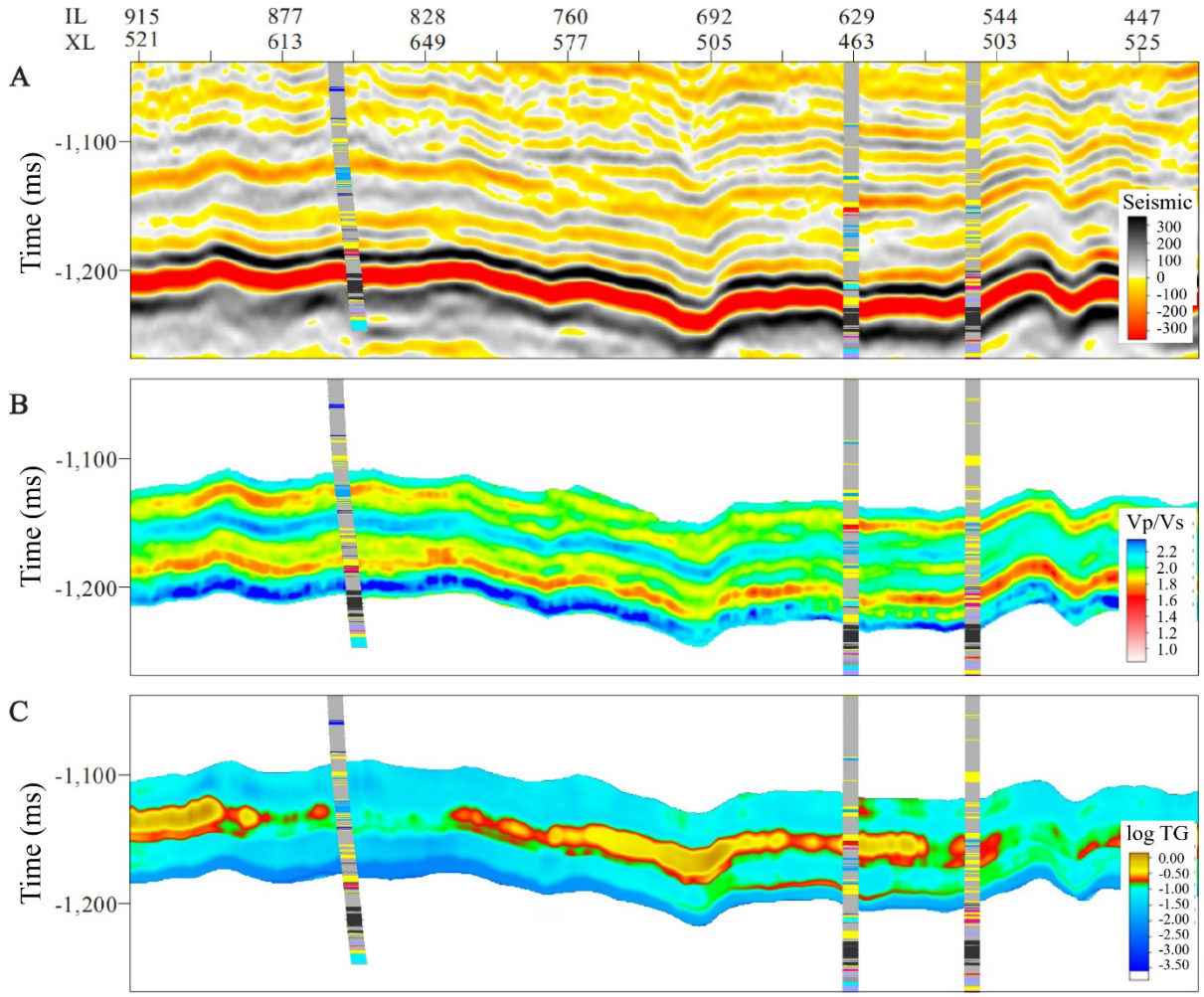

Figure 13. Prediction results of total gas (TG). (A) Seismic data. (B) Pre-stack P- and S-wave velocity ratio (Vp/Vs) obtained from pre-stack inversion. (C) TG prediction results, with red, blue, yellow, and gray at well locations representing gas layers, water layers, sandstone, and mudstone, respectively.

interpretation tasks, but pose high requirements on data input and model iterative maintenance.

(iii) The integration of prior geological and geophysical knowledge with ML models: Fundamental geological and geophysical understanding exerts a strong bias effect on ML models. In intelligent geophysical research, it is essential to fully integrate geologists' prior knowledge and domain expertise to ensure that models better simulate and predict real geological phenomena while maintaining a basic generalization ability. By incorporating geological logic into algorithm design, such as combining CRFs and path-optimization algorithms in horizon interpretation, both geological laws and the automation advantages of DL are considered. During model training, expert-curated, geologically significant labeled data are introduced to align predictions with geological reality, thereby enabling seamless integration of geological knowledge with intelligent algorithms.

5. Conclusion

This study presented a comprehensive, ML-driven workflow for seismic interpretation, applied and validated in the complex Linxing–Shenfu tight gas and CBM field. The key achievements are summarized as follows:

(i) An integrated intelligent workflow: We established and implemented a seamless, data-driven interpretation chain. This workflow systematically progresses from structural framework building through intelligent horizon and fault interpretation under low-SNR conditions to stratigraphic analysis via deep clustering for seismic facies and semantic segmentation of special geological bodies (e.g., the Zijinshan igneous rock mass).

(ii) Quantitative reservoir characterization: Leveraging deep learning models constrained by geological priors, this workflow successfully transitions from qualitative interpretation to quantitative prediction. It enables the direct and accurate estimation of key reservoir properties, including lithology, porosity, permeability, and gas saturation, culminating in the fine-scale, 3D characterization of composite geological "sweet spots."

(iii) Practical efficacy and broader implications: The application of this workflow has not only significantly enhanced interpretation efficiency and objectivity but has also effectively addressed persistent theoretical bottlenecks of conventional methods. These include managing low-SNR data, identifying thin interbeds, and resolving fluid ambiguity in complex rock physics scenarios. The success in the Linxing–Shenfu Block underscores the paradigm-shifting potential of integrated artificial intelligence-based workflows for unlocking the value of complex unconventional reservoirs, offering a robust and scalable template for efficient exploration and development decision-making in geologically analogous plays worldwide.

Acknowledgments

None.

Funding

None.

Conflict of interest

The authors declare no potential conflict of interest.

Author contributions

Conceptualization: Qixin Li
Formal analysis: Xiaowen Zheng, Bo Wang
Investigation: Di Wang, Jicai Ding
Methodology: Qixin Li
Writing–original draft: Wenlan Li
Writing–review & editing: Wenlan Li, Bo Wang

Availability of data

Data are available from the corresponding author upon reasonable request.

References

1. Liu JZ, Zhu GH, Liu YC, *et al*. Breakthrough, future challenges and countermeasures of deep coalbed methane in the eastern margin of Ordos Basin: A case study of Linxing-Shenfu block. *Acta Pet Sin*. 2023;44(11):1827-1839. [In Chinese].

   doi: 10.7623/syxb202311006

2. Mi L, Zhu G. Geological characteristics and exploration breakthrough in Linxing-Shenfu tight gas field, northeastern Ordos Basin. *China Pet Explor*. 2021;26(3):53-67. [In Chinese].

   doi: 10.3969/j.issn.1672-7703.2021.03.005

3. Wang SX, Yuan SY. *Ren gong zhi neng di qiu wu li kan tan. Artificial Intelligence for Geophysical Exploration*. Beijing: Science Press; 2025. [In Chinese].

4. Yu SW, Ma JW. Deep learning for geophysics: Current and future trends. *Rev Geophys*. 2021;59(3):e2021RG000742.

   doi: 10.1029/2021RG000742

5. Zhu YH, Zhao ZG, Lu YY, *et al*. Research progress and key technologies for exploration of onshore tight sandstone gas by CNOOC. *China Offshore Oil Gas*. 2024;36(6):13-25. [In Chinese].

doi: 10.11935/j.issn.1673-1506.2024.00.007

6. Zhu GH, Li BL, Li ZC, *et al*. Practices and development trend of unconventional natural gas exploration in eastern margin of Ordos Basin: Taking Linxing-Shenfu gas field as an example. *China Offshore Oil Gas*. 2022;34(4):16-29. [In Chinese].

   doi: 10.11935/j.issn.1673-1506.2022.04.002

7. Liu C, Zhang DM, Li C, Lu YY, Guo MQ. Upper Paleozoic tight gas sandstone reservoirs and main controls, Linxing block, Ordos Basin. *Oil Gas Geol*. 2021;42(5):1146-1158. [In Chinese].

   doi: 10.11743/ogg20210512

8. Ge Y, Zhu GH, Wan H, Pan XZ, Huang ZL. The influence of Zijinshan Structural belt to the formation and distribution of tight sandstone gas reservoir in Upper Paleozoic, in the eastern Ordos Basin. *Nat Gas Geosci*. 2018;29(4):491-499. [In Chinese].

   doi: 10.11764/j.issn.1672-1926.2018.03.008

9. Bergen KJ, Johnson PA, de Hoop MV, Beroza GC. Machine learning for data-driven discovery in solid Earth geoscience. *Science*. 2019;363(6433):eaau0323.

   doi: 10.1126/science.aau0323

10. Herron DA. Pitfalls in horizon autopicking. *Interpretation*. 2015;3(1):SB1-SB4.

    doi: 10.1190/INT-2014-0062.1

11. Hoyes J, Cheret T. A review of 'global' interpretation methods for automated 3D horizon picking. *Lead Edge*. 2011;30(1):38-47.

    doi: 10.1190/1.3535431

12. Wu XM, Fomel S. Least-squares horizons with local slopes and multi-grid correlations. *Geophysics*. 2018;83(4):IM29-IM40.

    doi: 10.1190/geo2017-0830.1

13. Xu YM. Di zhen pou mian duan ceng de jie shi yan jiu. Interpretation of faults in seismic profiles. *China Pet Chem Stand Qual*. 2012;33(10):50. [In Chinese].

    doi: 10.3969/j.issn.1673-4076.2012.10.040

14. Xi GM, He SG, Min Y, Sun YC, Li QC. Fault identification by the coherency attributes. *Northwest Geol*. 2019;52(1):244-249. [In Chinese].

    doi: 10.19751/j.cnki.61-1149/p.2019.01.023

15. Cai HP. Improvement of variance cube technique and its application in seismic interpretation. *Coal Geol Explor*. 2008;36(1):74-76. [In Chinese].

    doi: 10.3969/j.issn.1001-1986.2008.01.019

16. He Y, He ZH, Xiong XJ. Fault Identification Based on High-precision Curvature Analysis. *J Oil Gas Technol*. 2010;32(6):404-407. [In Chinese].

    doi: CNKI:SUN:JHSX.0.2010-06-102

17. Li HW, Bai XL, Cui JB, Wan HZ, Yuan SH, Chu WC. Fault identification technology of ant attribute optimization. *Coal Geol Explor*. 2019;47(6):174-179. [In Chinese].

    doi: 10.3969/j.issn.1001-1986.2019.06.026

18. Bi ZF, Wu XM, Geng ZC, Li HS. Deep relative geologic time: A deep learning method for simultaneously interpreting 3-D seismic horizons and faults. *J Geophys Res Solid Earth*. 2021;126(9):e2021JB021882.

    doi: 10.1029/2021JB021882

19. Geng ZC, Wu XM, Shi YZ, Fomel S. Deep learning for relative geologic time and seismic horizons. *Geophysics*. 2020;85(4):WA87-WA100.

    doi: 10.1190/geo2019-0252.1

20. Luo YL, Zhang GL, Li L, Zhang XD, Duan J, Li XW. Attention-based two-stage U-Net horizon tracking. *IEEE Geosci Remote Sens Lett*. 2022;19:1-5.

    doi: 10.1109/LGRS.2022.3217376

21. Wu XM, Liang LM, Shi YZ, Fomel S. FaultSeg 3D: Using synthetic data sets to train an end-to-end convolutional neural network for 3D seismic fault segmentation. *Geophysics*. 2019;84(3):IM35-IM45.

    doi: 10.1190/geo2018-0646.1

22. Li Y, Wu XM, Zhu ZY, Ding JC, Wang QZ. FaultSeg 3D plus: a comprehensive study on evaluating and improving CNN-based seismic fault segmentation. *Geophysics*. 2024;89(5):N77-N91.

    doi: 10.1190/geo2022-0778.1

23. Wei XL, Zhang CX, Kim SW, *et al*. Seismic fault detection using convolutional neural networks with focal loss. *Comput Geosci*. 2022;158:104968.

    doi: 10.1016/j.cageo.2021.104968

24. Li SZ, Liu NH, Li FY, Gao JH, Ding JC. Automatic fault delineation in 3-D seismic images with deep learning: Data augmentation or ensemble learning? *IEEE Trans Geosci Remote Sens*. 2022;60:1-14.

    doi: 10.1109/TGRS.2022.3150353

25. Zhou ZW, Rahman Siddiquee MM, Tajbakhsh N, Liang JM. UNet++: A Nested U-Net Architecture for Medical Image Segmentation. *arXiv*. Preprint posted online July 18, 2018. Accessed March 19, 2021.

    doi: 10.48550/arXiv.1807.10165

26. Liu BG, Liu LH. Application of Applied Seismic Sedimentology in Sedimentary Facies Analysis. *Geophys Prospect Pet*. 2008;47(3):266-271. [In Chinese].

    doi: 10.3969/j.issn.1000-1441.2008.03.010

27. Wrona T, Pan I, Gawthorpe RL, Fossen H. Seismic facies analysis using machine learning. *Geophysics*.

2018;83(5):O83-O95.

doi: 10.1190/geo2017-0595.1

28. Zhang LK, Qin LJ, Zhang GS, Sun XQ. On Seismic Facies Analysis Based on Seismic Attributes. *Chin J Eng Geophys*. 2010;7(6):694-698. [In Chinese].

doi: 10.3969/j.issn.1672-7940.2010.06.009

29. Barnes A. Redundant and useless seismic attributes. *Geophysics*. 2007;72(3):P33-P38.

doi: 10.1190/1.2716717

30. Yan XY, Gu HM, Luo HM, Yan YP. Intelligent Seismic facies classification based on an improved deep learning method. *Oil Geophys Prospect*. 2020;55(6):1169-1177. [In Chinese].

doi: 10.13810/j.cnki.issn.1000-7210.2020.06.001

31. Shuo LX, Zhao YH, Chai BF, Li ZH, Wu H. Semi-supervised adversarial network for seismic facies classification. *Prog Geophys*. 2023;38(5):2105-2113. [In Chinese].

doi: 10.6038/pg2023GG0372

32. Qian F, Yin M, Liu XY, Wang YJ, Lu C, Hu GM. Unsupervised seismic facies analysis via deep convolutional autoencoders. *Geophysics*. 2018;83(3):A39-A43.

doi: 10.1190/geo2017-0524.1

33. Liu ML, Jervis M, Li WC, Nivlet P. Seismic facies classification using supervised convolutional neural networks and semisupervised generative adversarial networks. *Geophysics*. 2020;85(4):O47-O58.

doi: 10.1190/geo2019-0627.1

34. Li QX, Luo YN, Ma XQ, Chen C, Zhu YH. Seismic facies clustering technology based on deep embedding network. *Oil Geophys Prospect*. 2022;57(2):251-260. [In Chinese].

doi: 10.13810/j.cnki.issn.1000-7210.2022.02.002

35. Wu XM, Yang JR, Zhu ZY, Ding JC, Wang QZ. Discussions on computational seismic structural interpretation and modeling. *Geophys Prospect Pet*. 2022;61(3):392-407. [In Chinese].

doi: 10.3969/j.issn.1000-1441.2022.03.002

36. Jones IF, Davison I. Seismic imaging in and around salt bodies. *Interpretation*. 2014;2(4):SL1-SL20.

doi: 10.1190/INT-2014-0033.1

37. Ronneberger O, Fischer P, Brox T. U-net: Convolutional networks for biomedical image segmentation. In: *Medical Image Computing and Computer-Assisted Intervention—MICCAI 2015*. Springer; 2015:234-241.

doi: 10.1007/978-3-319-24574-4_28

38. Shi YZ, Wu XM, Fomel S. Automatic salt-body classification using a deep convolutional neural network. In: *SEG Technical Program Expanded Abstracts 2018*. SEG International Exposition and Annual Meeting 2018; August 1, 2018. Society of Exploration Geophysicists; 2018:1971-1975.

doi: 10.1190/segam2018-2997304.1

39. Di HB, Wang Z, AlRegib G. Deep convolutional neural networks for seismic salt-body delineation. In: *Proceedings of the AAPG 2018 Annual Convention & Exhibition*. AAPG 2018 Annual Convention & Exhibition; May 20–23, 2018; Salt Lake City, Utah, United States. AAPG; 2018.

doi: 10.1306/70630Di2018

40. Shi YZ, Wu XM, Fomel S. SaltSeg: Automatic 3D salt segmentation using a deep convolutional neural network. *Interpretation*. 2019;7(3):SE113-SE122.

doi: 10.1190/INT-2018-0235.1

41. Yang XK, Yang YH, Ji LD, Su CQ, Zheng ML, Zhao L. Stages and characteristics of thermal actions in eastern part of Ordos Basin. *Acta Geol Sin*. 2006;80(5):705-711. [In Chinese].

doi: 10.3321/j.issn:0001-5717.2006.05.010

42. Yang XK, Chao HX, Zhang ZF, Yao WH, Dong M. Characteristics of the Zijinshan complex and its dynamic environment in the east of the Ordos Basin—Analysis of a classic example on the deep processes of thermal-magma activity in the basin. *Geotecton Metallog*. 2010;34(2):269-281. [In Chinese].

doi: 10.16539/j.ddgzyckx.2010.02.008

43. Chen G, Ding C, Xu LM, *et al*. Analysis on the thermal history and uplift process of Zijinshan intrusive complex in the eastern Ordos basin. *Chin J Geophys*. 2012;55(1):78-90. [In Chinese].

doi: 10.6038/j.issn.0001-5733.2012.11.020

44. Ren ZL, Zhang S, Gao SL, Cui JP, Xiao YY, Xiao H. E'erduosi pen di gou zao re yan hua shi ji qi cheng kuang cheng cang yi yi. Tectono-thermal evolution history of the Ordos Basin and its implications for hydrocarbon accumulation and mineralization. *Sci China Press*. 2007;37(suppl 1):23-32. [In Chinese].

45. Cooke DA, Schneider WA. Generalized linear inversion of reflection seismic data. *Geophysics*. 1983;48(6):665-676.

doi: 10.1190/1.1441497

46. Mukerji T, Avseth P, Mavko G, Takahashi I, Gonzalez EF. Statistical rock physics: combining rock physics, information theory, and geostatistics to reduce uncertainty in seismic reservoir characterization. *Lead Edge*. 2001;20(3):313-319.

doi: 10.1190/1.1438938

47. Avseth P, Mukerji T, Mavko G. *Quantitative Seismic Interpretation*. Cambridge University Press; 2005.

48. Grana D. Joint facies and reservoir properties inversion. *Geophysics*. 2018;83(3):M15-M24.

doi: 10.1190/GEO2017-0670.1

49. Grana D. Bayesian linearized rock-physics inversion. *Geophysics*. 2016;81(6):D625-D641.

doi: 10.1190/GEO2016-0161.1

50. Aleardi M, Ciabarri F. Application of different classification methods for litho-fluid facies prediction: a case study from the offshore Nile Delta. *J Geophys Eng*. 2017;14(5):1087-1102.

doi: 10.1088/1742-2140/aa7301

51. Larsen AL, Ulvmoean M, Omre H, Buland A. Bayesian lithology/fluid prediction and simulation on the basis of a Markov-Chain prior model. *Geophysics*. 2006;71(5):R69-R78.

doi: 10.1190/1.2245469

52. Wang L, Zhang F, Li XY, Di BR, Zeng LB. Quantitative seismic interpretation of rock brittleness based on statistical rock physics. *Geophysics*. 2019;84(4):IM63-IM75.

doi: 10.1190/geo2018-0094.1

53. Kong W, Zhang LJ, Cheng MW, Zhang HW, Jiang LZ. Application of Waveform Indication Inversion in the Prediction of Thin Carbonate Reservoirs in the Amu Darya Right Bank Area. In: Lin J, ed. *Proceedings of the International Field Exploration and Development Conference 2019*. IFEDC 2019; October 16–18, 2019; Xi'an, China. Springer; 2020:3256-3266.

doi: 10.1007/978-981-15-2485-1_302

54. Qi Y, Wu K, Wang B, Zheng XW, Li WL, Li D. Lithofacies identification of deep coalbed methane reservoir based on high-resolution seismic inversion. *Front Earth Sci*. 2024;12:1440729.

doi: 10.3389/feart.2024.1440729

55. Sena A, Castillo G, Chesser K, *et al*. Seismic reservoir characterization in resource shale plays: 'sweet spot' discrimination and optimization of horizontal well placement. In: *SEG Technical Program Expanded Abstracts 2011*. 81th SEG Annual International Meeting; September 18–23, 2011; San Antonio, Texas, United States. Society of Exploration Geophysicists; 2011:1744-1748.

doi: 10.1190/1.3627542

56. Hart BS, Pearson R, Rawling GC. 3-D seismic horizon-based approaches to fracture-swarm sweet spot definition in tight-gas reservoirs. *Lead Edge*. 2002;21(1):28-35.

doi: 10.1190/1.1445844

57. Le J, Jing YQ, Liang X, Fan HJ, Cai WT. Using seismic response characteristics to predict "sweet spot" locations in a low-permeability reservoir in the Bohai Sea. *Geophys Prospect Pet*. 2022;61(5):876-887. [In Chinese].

doi: 10.3936/j.issn.1000-1441.2022.05.012

58. Liu ZQ, Wang YM, Bai GC, Gong CL. Application of sweetness and its fusion attribute in the research of Deep-water reservoir. *Oil Geophys Prospect*. 2010;45(suppl 1):158-162.

doi: 10.13810/j.cnki.issn.1000-7210.2010.s1.005

59. Peng CZ, Peng J, Chen YH, Zhang HR. Seismic predicting of sweet spots in the Da'anzhai Shale Play, Yuanba area, Sichuan Basin. *Nat Gas Ind*. 2014;34(6):42-47. [In Chinese].

doi: 10.3787/j.issn.1000-0976.2014.06.007

60. Zhao C, Jin FM, Han GM, Guo SW, Xing X, Liu HZ. Direct prediction of sweet spots in sandstone reservoirs based on pre-stack probability inversion. *Oil Geophys Prospect*. 2023;58(5):1211-1219. [In Chinese].

doi: 10.13810/j.cnki.issn.1000-7210.2023.05.018

61. Qian YG. Application of machine deep learning technology in tight sandstones reservoir prediction: A case study of Xujiahe Formation in Xinchang, western Sichuan Depression. *Pet Reserv Eval Dev*. 2023;13(5):600-607. [In Chinese].

doi: 10.13809/j.cnki.cn32-1825/te.2023.05.007

62. Wang D, Zhang YM, Zhang FC, Ding JC, Niu C. Quantitative prediction of tight sandstone sweet spots based on deep learning method with prior information constraints. *Oil Geophys Prospect*. 2023;58(1):65-74. [In Chinese].

doi: 10.13810/j.cnki.issn.1000-7210.2023.01.006

63. An P, Cao DP. Ji yu tan xing zu kang he shen du xue xi de mi du yu ce fang fa yan jiu. Research on density prediction methods based on elastic impedance and deep learning. In: Proceedings of Annual Meeting of Chinese Geoscience Union 2018, October 21–23, 2018; Beijing, China. China Peace Publishing House; 2018:754-757. [In Chinese].

64. Zhang MG, Hong Z, Dou YT, Cui XJ. Application of time-frequency analysis technology to the gas detection in Sulige area. *Lithol Reserv*. 2013;25(5):76-85. [In Chinese].

65. Zhang YQ, Wang ZZ, Zhang N. Research on sand body identification and gas bearing area prediction of He 8 member in SU X Well Block of Sulige Gas Field. *Nat Gas Geosci*. 2011;22(1):164-170. [In Chinese].

66. Lin LM, Zheng Y, Shi H, *et al*. Gas-bearing prediction of thin tight sandstone reservoirs based on facies-controlled geostatistical pre-stack inversion: A case study of the middle Linxing Block in the Ordos Basin. *Nat Gas Ind*. 2023;43(2):56-66. [In Chinese].

doi: 10.3787/j.issn.1000-0976.2023.02.006

67. Deng BQ, Ding D. Reservoir prediction method based on seismic-gas logging fusion. *Mud Logging Eng*. 2025;36(1):77-84. [In Chinese].

doi: 10.3969/j.issn.1672-9803.2025.01.012

68. Song ZH, Yuan SY, Li ZM, Wang SX. KNN-based gas-

bearing prediction using local waveform similarity gas-indication attribute - An application to a tight sandstone reservoir. *Interpretation*. 2022;10(1):T1-T10.

doi: 10.1190/INT-2021-0045.1

69. Gao JH, Song ZH, Gui JY, Yuan SY. Gas-bearing prediction using transfer learning and CNNs: An application to a deep tight dolomite reservoir. *IEEE Geosci Remote Sens Lett*. 2022;19:3001005.

doi: 10.1109/LGRS.2020.3035568